Carbohydrate Polymers 91 (2013) 444–451

Contents lists available at SciVerse ScienceDirect

Carbohydrate Polymers

journal homepage: www.elsevier.com/locate/carbpol

Characterisation of large scale structures in starch granules via small-angle neutron and X-ray scattering

James Doutch, Elliot P. Gilbert*

Bragg Institute, Australian Nuclear Science and Technology Organisation, Locked Bag 2001, Kirrawee DC, NSW 2232, Australia

ARTICLE INFO

Article history:
Received 4 April 2012
Received in revised form 1 August 2012
Accepted 1 August 2012
Available online 9 August 2012

Keywords:
Starch
Small-angle neutron scattering
Small-angle X-ray scattering
Blocklets
Growth rings
Unified model

ABSTRACT

Small angle scattering (SAS) techniques have a distinguished track record in illuminating the semi-crystalline lamellar structure of the starch granule. To date, there have been few attempts to use SAS techniques to characterise larger-scale structures reported from imaging techniques such as growth rings, blocklets or pores, nor how these structures would modulate the well-known scattering arising from the semi-crystalline lamellar structure. In this study, SAS data collected over an extended q range were gathered from dry and hydrated starch powders from varied botanical sources. The use of neutrons and X-rays, as well as comparing dry and hydrated granules, allowed different levels of contrast in scattering length density to be probed and therefore selected structural regions to be highlighted. The lowest q range, 0.002–0.04 Å^{-1}, was found to be dominated by scattering from the starch granules themselves, especially in the dry powders; however an inflection point from a low contrast structure was observed at 0.035 Å^{-1}. The associated scattering was interpreted within a unified scattering framework with the inflexion point correlating with a structure with radius of gyration ~90 Å – a size comparable to small blocklets or superhelices. In hydrated starches, it is observed that there is an inflection point between lamellar and q^{-4} power-law scattering regions at approximately 0.004 Å^{-1} which may correlate with growth rings and large blocklets. The implications of these findings on existing models of starch lamellar scattering are discussed.

1. Introduction

Starch is the primary carbohydrate component in the human diet and the major storage polysaccharide in plants. Structurally it is deposited in a large number of granules which vary in dimension (~1–100 μm) according to botanical source (Jane, Kasemsuwan, Leas, Zobel, & Robyt, 1994). These granules are partially crystalline in nature containing alternating amorphous and semi-crystalline layers termed growth rings. The semi-crystalline layers consist of a lamellar arrangement of crystalline and amorphous regions with repeat distance of 90–100 Å that is readily detected in hydrated starch by small angle scattering (SAS) techniques, using X-rays and neutrons (SAXS and SANS) (Blazek & Gilbert, 2011; Cameron & Donald, 1992; Waigh, Gidley, Komanshek, & Donald, 2000). It is proposed that this occurs as the amorphous regions within the lamellar structure preferentially take up water and, as a result, an observable contrast in scattering length density between the crystalline and amorphous regions is achieved. However, in dry powders, the scattering associated with this lamellar peak is significantly decreased, as the intensity is largely based on intrinsic differences in physical density between the crystalline and amorphous regions (Cameron & Donald, 1992; Waigh et al., 2000). This is shown in Table 1 where the square of the contrast in scattering length density, for both neutrons and X-rays, for starch granules and their internal regions with respect to air and H_2O are summarised. X-ray powder diffraction techniques, characterising starch at spacing smaller than 1 nm demonstrate the presence of a number of different crystalline polymorphs at these length scales, such as the classic A- and B-type patterns. This shows considerable variance between granule species; for example, many cereal starches show A-type diffraction patterns, whereas the tuber and high amylose starch types often display B-type patterns (Buleon, Colonna, Planchot, & Ball, 1998).

The scattering from dry starch powders has not been studied in depth (Cameron & Donald, 1992; Waigh et al., 2000) and has been rationalised using two complementary approaches. The first assumes that there are three distinct scattering length densities within the granule (Cameron & Donald, 1992): corresponding to (i) crystalline and (ii) amorphous regions within the semi-crystalline lamellae and, surrounding these semi-crystalline lamellae, are (iii) amorphous growth rings. It is therefore assumed

* Corresponding author. Tel.: +61 2 9717 9470; fax: +61 2 9717 3606.
E-mail address: elliot.gilbert@ansto.gov.au (E.P. Gilbert).

0144-8617/$ – see front matter.
http://dx.doi.org/10.1016/j.carbpol.2012.08.002

Table 1
The square of the scattering contrast for SAXS and SANS of starch granules, assuming granule density 1.50 g cm^{-3}, amorphous fraction density 1.59 cm^{-3} and crystalline fraction density 1.72 g cm^{-3} (1).

	X-ray ($\times 10^{20}$ cm^{-4})	Neutron ($\times 10^{20}$ cm^{-4})
Overall granule to air	182.3	3.08
Overall granule to water	16.66	5.36
Crystalline fraction (hydrated) to water	36.74	6.62
Amorphous fraction (hydrated) to water	23.93	5.86

that if the starch granules are not hydrated in excess water, there is insufficient contrast between the amorphous and crystalline regions for the lamellar peak to be observed with respect to the surrounding amorphous growth ring. The second approach considers starch to act as a liquid crystal, with hydration enabling sufficient chain mobility to occur such that a proportion of the amylopectin branches are able to align (Waigh et al., 2000). Conversely, in the absence of water, the branches exhibit greater disorder and lamellar scattering is reduced. This is often considered within the formalism of nematic and smectic behaviour – in the smectic state helices are aligned into lamellae, with this breaking down into a laterally non-aligned, smectic, state.

These structural models provide satisfactory fits for the lamellar peak, however do not account for scattering observed at q values below the lamellar peak, i.e. <~0.04 Å^{-1} (Blazek & Gilbert, 2010, 2011). This may imply that the SAS patterns are modulated at these q-ranges by other larger scale structures not accounted for in a purely lamellar description. For example, Cameron and Donald (1992) interpret the scattering from potato starch to be associated with semi-crystalline growth rings that, on average, contain ca. 16 lamellar layers of approximately 90 Å each, giving a total thickness of ca. 1440 Å. However, such large-scale structures would be expected to influence the scattering pattern down to ca. 0.004 Å^{-1}. Surface pores are thought to have diameter of 20–30 Å (Sujka & Jamroz, 2010); scattering from these structures is likely to be masked by lamellar scattering. However, a population of larger cavities or macroscopic pores of dimension 1000–2000 Å may occur around certain granules, which could affect scattering in the range ca. 0.006–0.003 Å^{-1}. The influence of pores may become increasingly significant in the scattering from starch granules subject to enzymatic hydrolysis.

The use of imaging techniques, such as atomic force microscopy, on starch granules has suggested the presence of an intermediate level of order within the starch granule that is not accounted for within existing scattering frameworks. These are referred to as blocklets and are believed to form spheroidic structures within the growth rings. Reported dimensions of these structures are in the range 150–5000 Å and which appear to vary in location within a granule and with botanical source (for review see Perez & Bertoft, 2010; Tang, Mitsunaga, & Kawamura, 2005). Other substructures which may plausibly modulate the scattering pattern are superhelices (Oostergetel & van Bruggen, 1993).

In this study we utilised SAXS and SANS to investigate the scattering from starch in the form of 'dry' powders (i.e. those at their ambient, native hydration ~15%) and from fully hydrated starch slurries (using H_2O for both X-ray and neutron studies) to investigate the low q scattering under different contrast conditions in the context of considering the influence of structures in the starch granule on larger length scales than lamellae. One key advantage of the use of SANS and SAXS techniques is the minimal sample preparation required, and in particular the ability to avoid fixatives and penetrating resins.

2. Materials and method

2.1. Small angle X-ray scattering (SAXS)

SAXS measurements were performed on a Bruker Nanostar with rotating anode source operated at wavelength, λ of 1.54 Å (Cu K_α) with a sample-to-detector distance of 115.5 mm, and beam size 0.5 mm, giving q range from 0.005 to 0.22 Å^{-1} using a Vantec 2000 2D area detector, where q is the magnitude of the scattering vector defined as:

$$q = \frac{4\pi}{\lambda} \sin\,\theta \tag{1}$$

and where 2θ is the scattering angle.

Native starch powders from tapioca (Penford, AU), maize (Penford, NZ), waxy maize (Tate and Lyle, Decatur, IL), high amylose maize (Hylon VII, Penford, AU), potato, and wheat (both commercial material, supermarket, Sydney, AU) were presented in 2 mm quartz capillaries (Hilgenburg Gmbh, Germany) as both 'dry' powders at ambient hydration levels and as hydrated slurries under excess water to the X-ray beam. The scattering patterns were reduced and radially averaged with Bruker software. A scattering background from an empty quartz capillary, or quartz capillary filled with water, were subtracted as appropriate, after correction for sample transmission. X-ray data were placed on an absolute scale using water as a standard (Fan, Degen, Bendle, Grupido, & Ilvasky, 2010). These operations were performed using the IRENA macro suite for manipulating and analysing SAS data (Ilavsky & Jemian, 2009) within the Igor analysis package (Wavemetrics, Lake Oswego, OR). We note, however, that absolute intensity values are highly influenced by the packing density of the samples which is ill-defined.

2.2. Small angle neutron scattering (SANS)

SANS experiments were performed on the 40 m Quokka instrument at the OPAL reactor; this instrument has been described previously (Gilbert, Schulz, & Noakes, 2006). Four configurations were used to cover a q range 0.0005–0.7 Å^{-1}. Three of these were 'standard' configurations: (i) source-to-sample distance (SSD) = 9.965 m, sample-to-detector distance (SDD) = 1.354 m, (ii) SSD = 3.949 m, SDD 4.044 m and (iii) SSD = 20.245 m, SDD = 20.094 m using a wavelength of 5.034 Å and 14% wavelength resolution and with source and sample aperture diameters of 50 mm and 10 mm, respectively. To access lower q values, a focussing optics configuration was used in which an array of 24 MgF_2 lenses were employed to focus neutrons at the detector with wavelength 8.1 Å; in this approach, minimum q is determined by the size of the image of the source aperture at the detector. As with the SAXS measurements, both dry and hydrated samples were investigated, having first been placed in 1 mm path length cells with demountable quartz windows.

SANS data were reduced using NCNR SANS reduction macros (Kline, 2006) modified for the Quokka instrument in Igor. Background subtraction and sample transmission corrections were performed using an empty cell or a cell of water as appropriate. Data were then transformed to absolute scale by the use of an attenuated direct beam transmission measurement.

2.3. Data analysis

SAXS and SANS data were plotted in the IRENA package (Ilavsky & Jemian, 2009). Selected data are displayed in the form of $I(q)q^4$ plots to emphasise deviations from Porod-type scattering (i.e. $I(q) \sim q^{-4}$) arising from granule–solvent or granule–air interfaces. Data were analysed using the Beaucage Unified fit method (Beaucage, 1996) as outlined in Section 4 and coded within the NIST analysis macro suite (Kline, 2006).

3. Results

3.1. SAXS data

Fig. 1a shows the SAXS for dry powders on an absolute scale. In several starches, a lamellar interference peak can be seen at approximately 0.07 Å^{-1}. This occurs at 0.09 Å^{-1} in the waxy maize sample. Potato was the only exception from showing an interference peak. At lower q, a strong interfacial scattering regime is observed which is modulated in all starches by an inflection which appears to be centred at 0.03 Å^{-1}. The Potato SAXS has the lowest absolute intensity. By calculating the Porod constant at the lowest q values, under the limiting assumption of q^{-4} behaviour, it can be demonstrated that this is due to the lower surface area per unit volume (~900 cm^{-1} for potato, ~2600 cm^{-1} for maize); this is consistent with larger mean granule size in potato compared to the other starches studied here (Jane et al., 1994).

Fig. 1b shows SAXS data from hydrated starches. Here the lamellar interference peak centred at approximately 0.06 Å^{-1} is very prominent in the log–log plot (in contrast to the powder samples), with power law scattering (between −2 and −3) behaviour observed at lower q values.

3.2. SANS data

Neutron scattering measurements from dry powders are shown in Fig. 2a. The region below 0.02 Å^{-1} in reciprocal space appears to be dominated by interfacial scattering. At higher q, the signal is increasingly dominated by incoherent background scattering arising primarily from hydrogenous material in the systems studied.

SANS data from hydrated starch powders are shown in Fig. 2b. Here, a lamellar peak is observed, as per the SAXS measurements above. The q range extension available on the Quokka instrument also allows the interhelix peak (Perry & Donald, 2000) to be observed in the potato and high amylose starches as is expected for B-type crystallinity. At q values below the lamellar peak, there appear to be two power law regimes linked by an inflection point that occurs at approximately 0.0045 Å^{-1}.

4. Discussion

4.1. Dry powders

The lamellar peak in dry powders appears to be displaced towards higher q (i.e. lower d-spacing) from the usual position found in hydrated samples, presumably due to a lack of granule swelling which would accompany full hydration. Waxy maize, in particular, is displaced to around 0.09 Å^{-1} implying lamellar d-spacing of ~76 Å (see Table 2a). The lamellar peak appears to be absent in the dry potato starch powder, one of only two B-type starches used in this study.

In all of the dry starch powders there is an inflexion point observed below the lamellar peak, around 0.03 Å^{-1} but whose position does not appear to depend on the position of the lamellar peak. This is analysed using a combination of the unified model (Beaucage, 1996) and a Lorentzian peak function at higher q. This allows combinations of multiple power law and Guinier regions within one equation. Here, the Lorentzian function was added to account for the lamellar interference peak. Each unified level is characterised by a power law, the power law prefactor B and, if needed, an associated Guinier region of radius R_g and prefactor G (Beaucage, 1996), given in Eq. (2). The prefactors G and B are highly dependent on the geometry of the scattering object and are applicable both to classical particles, such as rods and platelets, and branched or chain like fractal aggregates (Beaucage, 1996, 2004).

$$I(q) = G\exp\left(-\frac{q^2R_g^2}{3}\right) + B\left\{\frac{\left[erf\left(qR_g/\sqrt{6}\right)\right]^3}{q}\right\}^P \quad (2)$$

The fitting parameters for the SAXS data on starch powders are shown in Table 2a. The lamellar interference peak shows considerable botanical variation in position. It is particularly interesting to note the difference between the waxy and normal maize. The Guinier region around 0.03 Å^{-1} appears to correlate to a structure with radius of gyration 87–99 Å. There are small botanical variations; however, these do not appear to be as significant as the changes in the lamellar peak position. The underlying power law regimes are greater than −3 in all cases, suggesting a surface fractal structure with little influence of botanical origin. Although there is considerable natural variation in starch granule size, the differences are only significant on length scales far outside the conventional range of small-angle scattering techniques (Blazek & Gilbert, 2010). It can be speculated that differences in granule surface porosity is likely to manifest itself as a change in the power law regime (Brenner, Adkins, Spooner, & Davis, 1995; Radlinski et al., 2004), however a larger sample set across a much wider botanical range would be needed to address this appropriately. Representative fits are shown in Fig. 3 for maize and potato starch.

From the relationship between the Guinier and power law prefactors, G and B, determined by fitting, a spherical form can be deduced (Beaucage, 1996; Beaucage, Kammler, & Pratsinis, 2004). The Guinier radii detected here are then likely to correlate to a structure which has diameter ~250 Å (assuming monodispersity for such spherical objects). The radius of gyration is within the lower limits proposed for the 'blocklet' structures detected by other methods (Baker, Miles, & Helbert, 2001; Szymonska & Krok, 2003). This structure appears to be present in all the starches investigated.

There are known to be significant variations in blocklet size from starches of different botanical origin (see Perez & Bertoft, 2010 for review). It is possible that the scattering detected here has its origin in some of the smaller building blocks present in all starch granules, from which larger blocklets are built up, such as superhelices, with the latter thought to have dimensions of 180 Å (Oostergetel & van Bruggen, 1993); however, the relationship between blocklets and superhelices is at present rather unclear (Bertoft, 2004; Perez & Bertoft, 2010). The scattering from larger blocks or zones is likely to be masked by interfacial surface scattering in this instance. Neutron data from dry powders showed an interfacial scattering regime below 0.01 Å^{-1}; beyond this point, intense background scattering is observed that masks any possible Guinier region (see Fig. 2a). This strong background almost certainly has its origin in the incoherent scattering from hydrogen atoms in the starch. The interfacial scattering from the dry samples with neutrons is less intense than that seen with X-rays. This is presumably due to the much lower granule contrast for neutrons, calculated to be 1.814×10^{-6} Å^{-1} – many times smaller than that for X-rays 13.95×10^{-6} Å^{-1} (Blazek & Gilbert, 2011).

4.2. Hydrated material

The scattering data from starch samples hydrated in excess water consisted of power law q dependencies modulated by the well-known peak arising from the lamellar structure (e.g. Blazek & Gilbert, 2011; Cameron & Donald, 1992) and its higher order reflections, if present.

Displaying the hydrated samples on a Porod plot ($I(q)q^4$ versus q) can highlight differences in power law dependence as a function of q; in particular, it is of interest to determine the point at

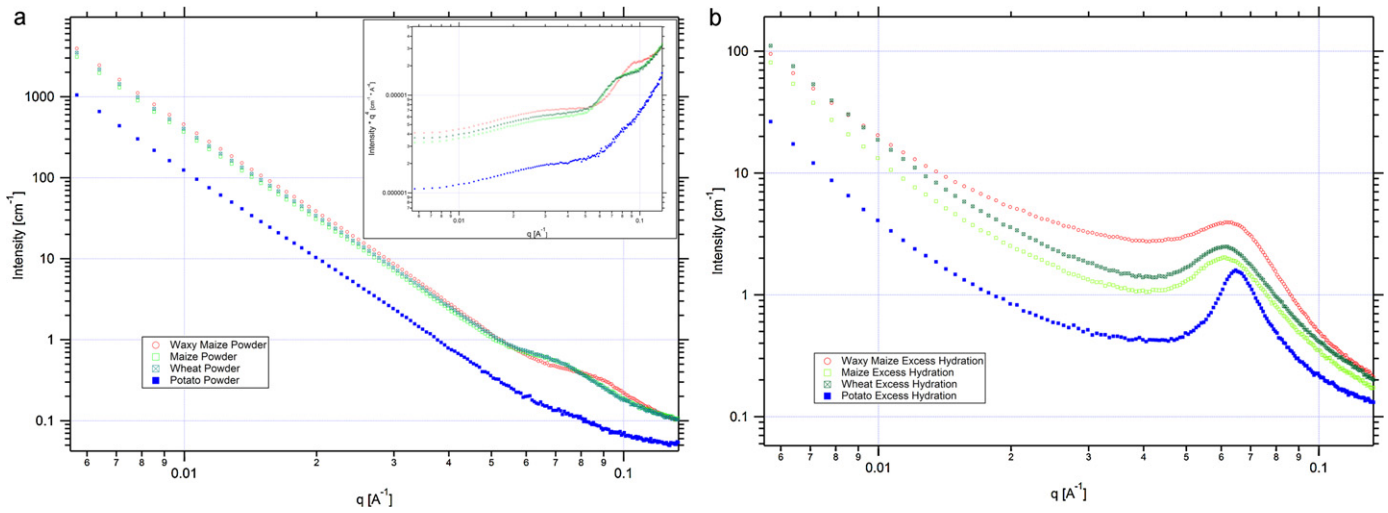

Fig. 1. Comparison of SAXS data from (a) dry powder starches; inset shows inflection region enlarged on Porod plot; (b) hydrated starch powders.

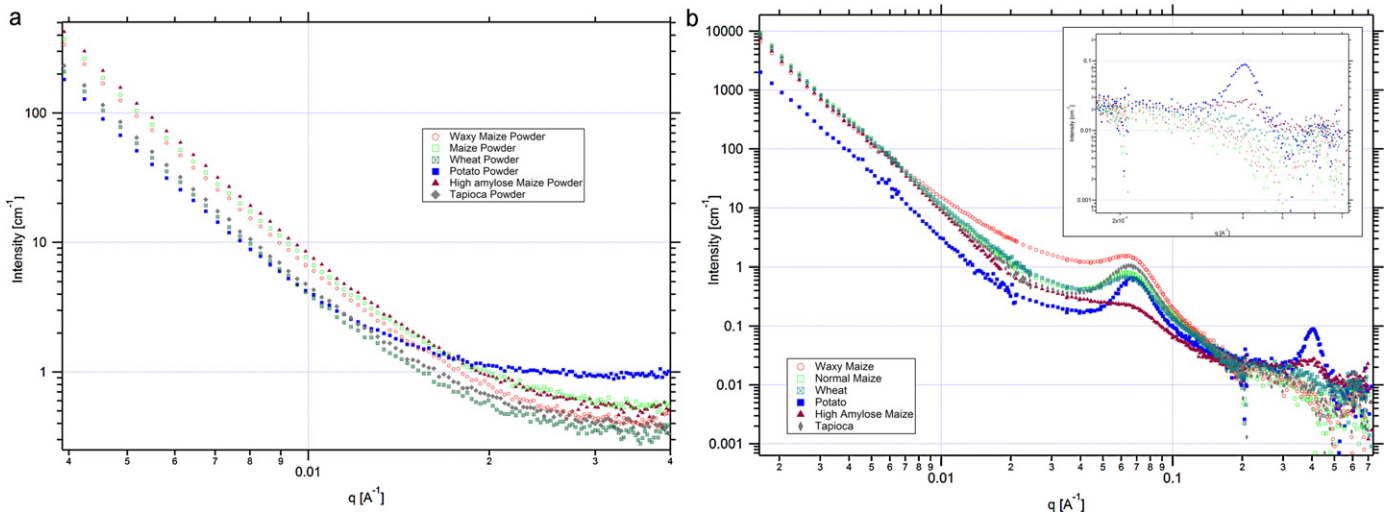

Fig. 2. SANS measurements from (a) dry starch powders and (b) hydrated starches (inset shows interhelix peak).

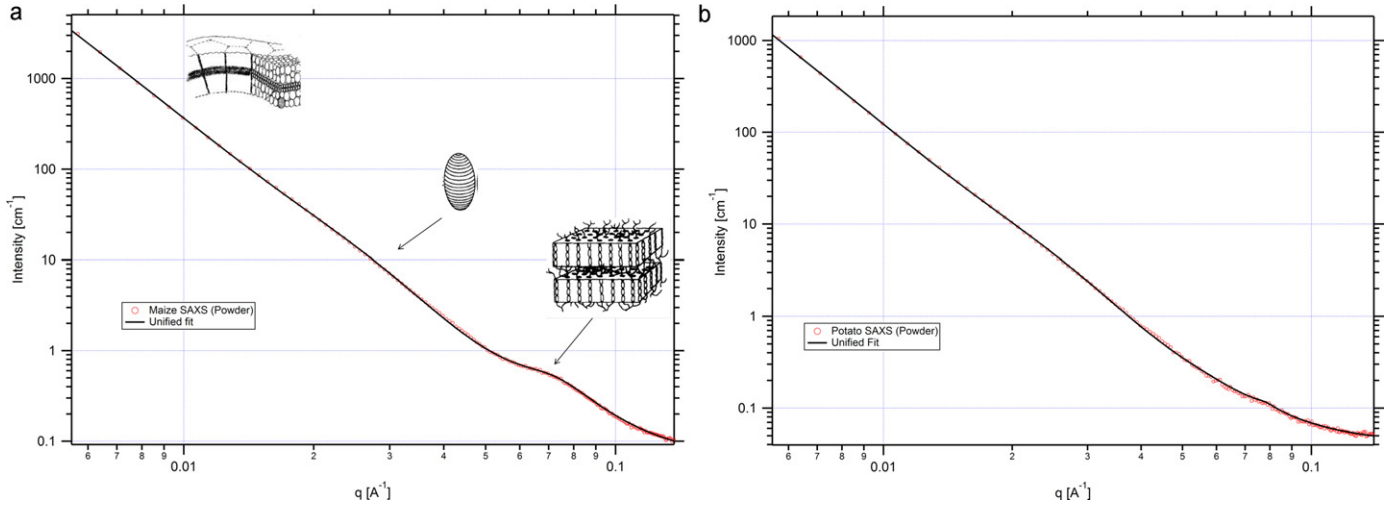

Fig. 3. SAXS from (a) maize and (b) potato starch (dry powders) with corresponding fits to the data using unified model plus Lorentzian peak function. Structural diagrams in (a) reprinted from Gallant et al. (1997), with permission from Elsevier.

Table 2a
Unified fitting parameters for dry starch powders (values in parentheses denote one standard deviation, 1st level covers q-range ~0.006~0.01, 2nd level q-range ~0.01~0.05).

	Maize	Potato	Waxy maize	Wheat
B (1st level)	$2.83(2) \times 10^{-05}$	$6.46(1) \times 10^{-06}$	$2.78(2) \times 10^{-05}$	$2.50(2) \times 10^{-05}$
Power law (1st level)	3.59(1)	3.670(2)	3.64(1)	3.64(2)
G (2nd level)	46.9(5)	23.6(4)	94(1)	76(3)
R_g (Å) (2nd level)	86.7(3)	96.1(5)	98.7(3)	96.6(8)
B (2nd level)	$1.72(2) \times 10^{-05}$	$6.56(2) \times 10^{-06}$	$8.83(2) \times 10^{-06}$	$6.7(2) \times 10^{-06}$
Power law (2nd level)	3.64(5)	3.61(6)	3.9(3)	3.98(2)
Peak intensity	0.22(4)	0.011(1)	0.16(2)	0.24(5)
Peak position ($Å^{-1}$)	0.070(1)	0.078(1)	0.083(1)	0.069(3)
Peak hwhm ($Å^{-1}$)	0.018(2)	0.006(2)	0.018(1)	0.018(3)
Bgd (cm^{-1})	0.062(1)	0.042(3)	0.061(3)	0.065(1)
Reduced Chi	5.7	2.2	5.8	5.6

which the lamellar q dependence, classically indicated by power law slope of q^{-2}, transitions to interfacial scattering, at lower q values. Previous analysis of SAXS measurements from starch granules of various botanical origin (waxy/normal maize, tapioca, potato) using paracrystalline models have suggested that the lamellar stack contains approximately 16–25 repeats, N (Daniels & Donald, 2003), and this appears to be consistent with electron microscopy (Gallant, Bouchet, & Baldwin, 1997). Therefore, the total height of a semi-crystalline lamellar stack should be of the order of 1500–2500 Å, which is at the edge of the detectable range of our X-ray data but well within the range of the SANS data.

Fig. 4 appears to demonstrate the existence of an inflection point between two power law regimes. A randomly oriented, dilute system of lamellae would have a q^{-2} dependence (Beaucage, 1996). It is observed that the power law dependence follows an approximate q^{-2} relation until q ~0.01–0.02 $Å^{-1}$; in Fig. 4(a) this is plotted as a Kratky plot for the hydrated starches with the behaviour also amply demonstrated by the Porod plot in Fig. 4(b). It would appear that the q dependence of the starch scattering changes markedly in this region, possibly into an interfacial scattering regime, however our SAXS data do not cover sufficient range to make a definitive elucidation. The SAXS and SANS data however show good agreement on an absolute scale and tend to converge for all starches close to 0.01 $Å^{-1}$, the difference at higher q-values certainly being related to incoherent scattering from hydrogens in the neutron case. The intensity differences on absolute scale show excellent agreement with calculated contrasts (Table 1).

The inflection point substructure peak is not observed around 0.03 $Å^{-1}$ in the hydrated samples. This region is presumably affected by the high electron contrast between the crystalline and amorphous lamellae as a result of starch hydration. The hydrated samples were also analysed using the unified model as for the powder samples (Beaucage, 1996) as shown in Tables 2b and 2c.

If the data are fitted assuming an interference function and either one or two power law regimes with no Guinier regions, the fitting in the region 0.03–0.05 $Å^{-1}$ is found to be inadequate, particularly in waxy maize and potato. It was hypothesised that this region may be perturbed by underlying structures such as blocklets or superhelices. The SAXS data suggest that the superior fits are obtained by allowing an underlying Guinier region close to the lamellar interference function of radius of gyration ~50 Å. Fits are shown in Figs. 5 and 6 for maize and potato, using SAXS and SANS respectively. This is rather smaller than the dimension detected in the dry powders; the relationship between the prefactors B and G indicate that this is scattering from a different object, a relatively flat or platelet-like structure. Such a Guinier feature is not necessary to fit this region in the neutron data, however, presumably due to the difference in contrast. In understanding this region, it is instructive to consider the scattering from 'plates' of lamellae. If it is asserted that starch is composed of superhelices and/or blocklets then the lamellae must have finite lateral dimensions. It is therefore expected that, under certain contrast conditions, these structures would manifest themselves as structures with two radii of gyration and it is likely this is what this region represents and contrary to models assuming infinite lateral spatial extent. There are relatively small differences detected between lamellar peak positions in SAXS and SANS measurements; these are likely to be caused by small hydration differences between samples since instrumental resolution was accounted for during analysis of neutron data. It is noted that the width of the lamellar peak in Hylon VII is broader than that of the other starches studied. Wellner et al. recently reported that *ae* mutant maize starch granules exhibit a significantly more heterogeneous intragranular structure than wild type maize (Wellner, Georget, Parker, & Morris, 2011). It is possible that the broader lamellar peak observed has its origin in such heterogeneity.

There are also differences in power law behaviour between the neutron and X-ray case. This is almost certainly caused by differences in contrast in internal structures between X-rays and neutron sources. There are very small variations observed between experimental data and the unified fitting model in the transition zone between two levels (for example, ~0.02 $Å^{-1}$ in Fig. 5a); this is likely caused by insufficient damping of power law behaviour at the termination of structural levels originating from the same object. Additionally, it should be noted that the SAXS data do not extend to as low a q value as the SANS data; this more limited range will presumably affect the fitted values of the terminal power law.

The extended q range obtained through SANS measurements illuminates an inflection region not observed in the SAXS spectra. Both indicate the presence of surface fractal scattering at very low q values. This is fitted using the unified model and indicates a nanometre scale (0.005–0.040 $Å^{-1}$) structure with botanical variance, unlike any of the structures discussed previously. It is of note that this inflection represents a transformation in power law behaviour from that indicative of a mass fractal or lamellar (−1 to −3) structure into that of a rough surface, presumably arising from interfacial scattering from granules and/or growth rings (−3 to −4). As such, it may represent scattering from large blocklets or the largest region of organisation within the branching structure of the growth rings. The values, in particular, are somewhat close to those of larger blocklets (Baker et al., 2001; Szymonska & Krok, 2003). The strong botanical variation strengthens the hypothesis that this represents blocklet scattering. This is not seen in dry powders due to intense scattering from the granule surface.

In terms of variations between starch varieties, the structures in waxy starch have the smallest radius of gyration. This implies that there are no large blocklets or, as far as a fractal structure is concerned, that correlations within the branching structure do not extend very far. High amylose maize has a relatively large substructure.

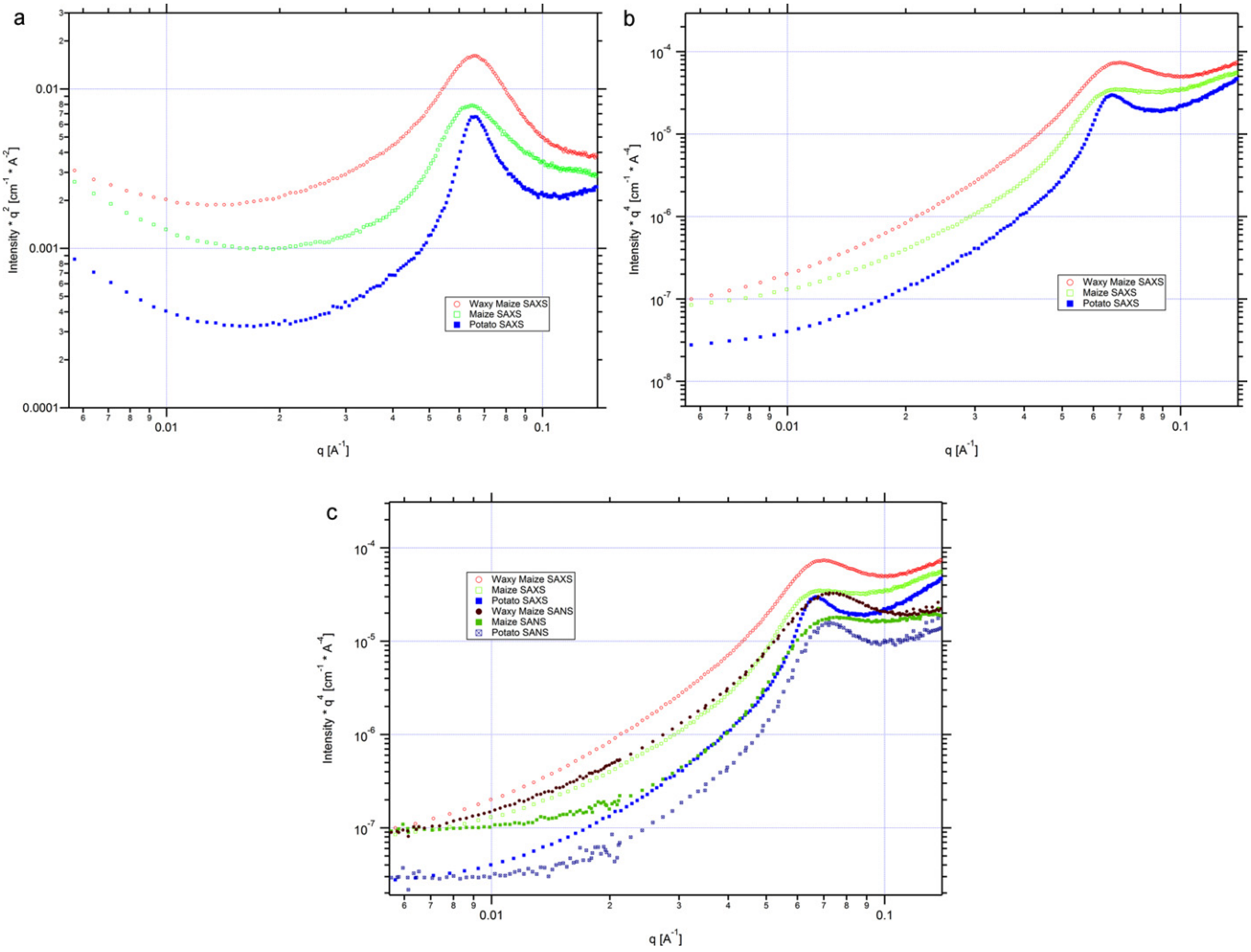

Fig. 4. Plot of (a) $I(q)q^2$, SAXS (b) $I(q)q^4$, SAXS and (c) combined plot of X-ray and neutron data on Porod plot for starch granules in excess water (selection of samples shown for clarity).

The analysis presented here (Tables 2a and 2b) strongly suggests detectable differences in surface fractal behaviour; this may also imply detectable differences in porosity (Huber & BeMiller, 2000; Sujka & Jamroz, 2010). The SAXS from native powders exhibit minor differences in power law behaviour; however, all samples indicate a relatively rough surface fractal dimension. In the hydrated case, in which the contrast of the granule surface is substantially lowered, there are detectable differences between starches that may elucidate the topology of growth rings, blocklets and the granule surface. In turn, the surface fractal region is likely to be affected by a rather complex mixture of granule size, distribution, surface roughness, and porosity, and the relative contrast of these structures under neutron and X-ray scattering. A study investigating the influence of different solvents using this approach would be of interest following seminal work by Perry and Donald (2002).

Table 2b
Unified fitting parameters for starch under excess hydration with SAXS (values in parentheses denote one standard deviation, 1st level covers q-range ~0.006~0.015, 2nd level q-range ~0.015~0.04).

	Maize	Potato	Waxy maize	Wheat
B (1st level)	$4.42(1) \times 10^{-06}$	$8.10(4) \times 10^{-07}$	$2.47(8) \times 10^{-05}$	$9.24(3) \times 10^{-06}$
Power law (1st level)	3.23(1)	3.34(1)	2.92(1)	3.15(1)
G (2nd level)	1.9(1)	0.54(1)	3.7(1)	2.6(1)
R_g (Å)	51.9(3)	44.1(2)	37.7(5)	52.4(2)
B (2nd level)	$1.36(3) \times 10^{-03}$	$8.59(3) \times 10^{-03}$	$4.91(2) \times 10^{-03}$	$1.85(4) \times 10^{-03}$
Power law (2nd level)	2.18(1)	2.15(2)	1.37(2)	2.10(1)
Peak intensity	1.550(2)	1.315(6)	3.286(2)	1.934(2)
Peak position ($Å^{-1}$)	0.062(5)	0.066(2)	0.063(3)	0.062(3)
Peak hwhm ($Å^{-1}$)	0.0121(1)	0.0072(5)	0.0135(9)	0.0120(1)
Bgd (cm^{-1})	0.012(4)	0.052(5)	0.020(1)	0.012(5)
Reduced Chi squared	2.1	2.3	2.1	2.0

Table 2c
Unified fitting parameters for starch under excess hydration with SANS (values in parentheses denote one standard deviation, values in parentheses denote one standard deviation, 1st level covers q-range ~0.003~0.02, 2nd level q-range ~0.02~0.04).

	Maize	Potato	Waxy maize	Wheat	Tapioca	Hylon
B (1st level)	$9.3(6)\times10^{-07}$	$8.7(1)\times10^{-07}$	$5.49(2)\times10^{-06}$	$1.33(9)\times10^{-06}$	$1.31(9)\times10^{-06}$	$2.4(4)\times10^{-06}$
Power law (1st level)	3.56(1)	3.35(2)	3.19(1)	3.49(1)	3.50(1)	3.38(3)
G (2nd level)	15(1)	3(1)	5.0(0.1)	20(1)	14(1)	52(5)
R_g (Å)	180(3)	180(10)	88(1)	186(3)	184(3)	263(4)
B (2nd level)	$1.16(2)\times10^{-03}$	$3.0(4)\times10^{-03}$	$8.2(9)\times10^{-05}$	$5.5(7)\times10^{-04}$	$9.3(9)\times10^{-04}$	$4.4(7)\times10^{-04}$
Power law (2nd level)	1.66(1)	1.16(4)	3.00(3)	1.91(3)	1.61(2)	1.84(4)
Peak intensity	0.798(2)	0.823(4)	1.488(5)	0.610(2)	1.637(3)	0.168(3)
Peak position ($Å^{-1}$)	0.06458(3)	0.06828(3)	0.06427(4)	0.06402(4)	0.06548(2)	0.0585(2)
Peak hwhm ($Å^{-1}$)	0.01311(7)	0.00665(6)	0.01084(8)	0.01270(1)	0.01027(5)	0.0206(5)
Incoherent Bgd (cm^{-1})	−0.001(1)	0.004(2)	0.001(3)	0.006(1)	0.003(1)	0.007(5)
Reduced Chi squared	3.3	2.5	5.9	3.6	2.8	4.0

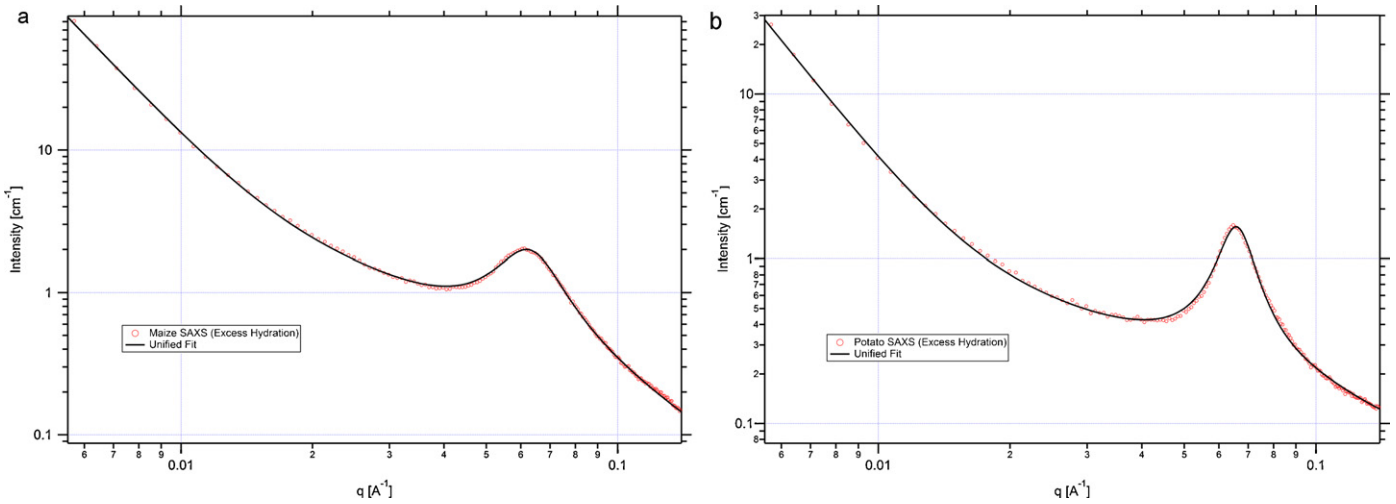

Fig. 5. SAXS data from starch samples under excess water (a) maize and (b) potato showing corresponding data fits from unified model.

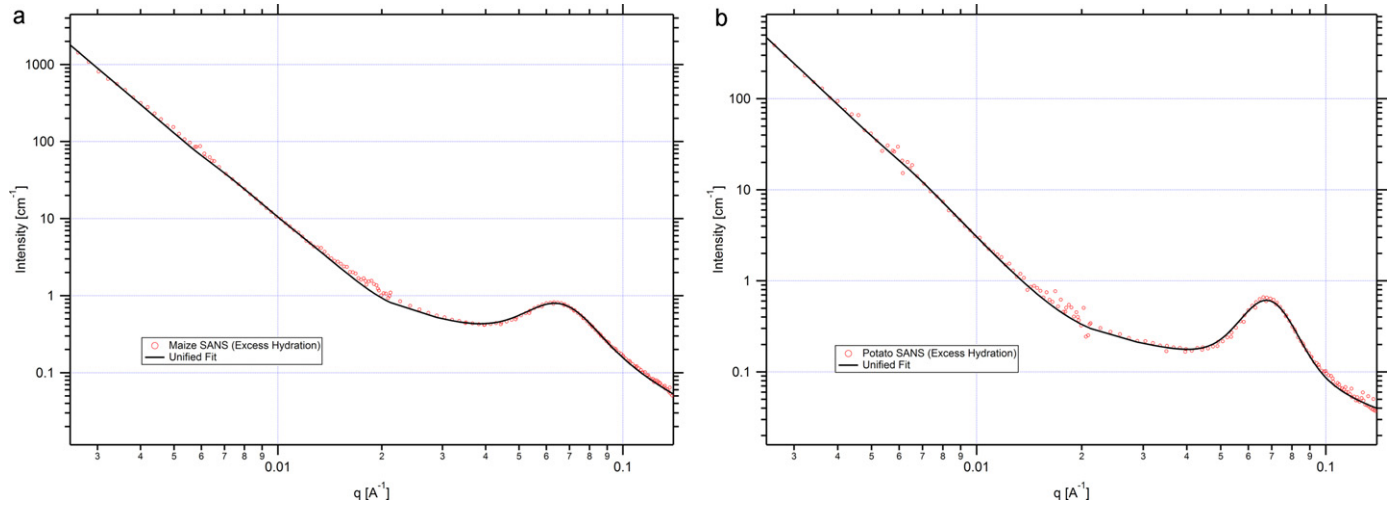

Fig. 6. SANS data showing corresponding fits from unified model under excess water for (a) maize and (b) potato.

5. Conclusions

Small-angle scattering data from starch granules has traditionally been fitted using models that assume a lamellar structure of infinite lateral spatial extent, or using power law plus peak fitting methods. Here, a new methodology based on the semi-empirical unified approach is used that not only better describes the observed scattering over an extended q range but that is also shown to highlight the scattering from putative blocklet, superhelix and fractal structures. It is demonstrated that SAXS on native starch powders illuminates the presence of a surface fractal regime and, furthermore, appears to contain scattering arising from blocklets or superhelices; structures that have not been characterised by SAS methods previously. The use of SANS and SAXS techniques allows a variety of q-ranges and contrasts to be probed and, in the hydrated samples, where scattering from the granule surface is significantly diminished, a larger dimension substructure is detected, which shows considerable botanic variation.

As SAS methods require minimal sample preparation and probe the material in the native state, the data presented here appear not only to confirm the existence of higher order structures between lamellae and growth rings that have been proposed from various microscopy techniques and across a wide botanic variety of starch granules, but also without the influence of possible artefacts from sample preparation. In addition, due to the significantly greater probe volume compared to microscopy techniques, these scattering methods also have the advantage of yielding data that are representative of the bulk average structure.

Further work with the unified methodology is appropriate to examine how generally applicable this is to a broader range of native starches, and whether it can also be employed to analyse data from processed systems, e.g. during Rapid Visco Analysis (Doutch et al., 2012) or digestion (Blazek & Gilbert, 2010; Wang, Blazek, Gilbert, & Copeland, 2012).

References

Baker, A. A., Miles, M. L., & Helbert, W. (2001). Potato starch granule nanostructure studied by high-resolution non-contact AFM. *International Journal of Biological Macromolecules*, *33*, 1–7.

Beaucage, G. (1996). Small-angle scattering from polymeric mass fractals of arbitrary mass-fractal dimension. *Journal of Applied Crystallography*, *29*, 134–146.

Beaucage, G. (2004). Determination of branch fraction and minimum dimension of mass-fractal aggregates. *Physical Review E*, *70*, 031401.

Beaucage, G., Kammler, H. K., & Pratsinis, S. E. (2004). Particle size distributions from small-angle scattering using global scattering functions. *Journal of Applied Crystallography*, *37*, 523–535.

Bertoft, E. (2004). On the nature of categories of chains in amylopectin and their connection to the super helix model. *Carbohydrate Polymers*, *57*, 211–224.

Blazek, J., & Gilbert, E. P. (2010). Effect of enzymatic hydrolysis on native starch granule structure. *Biomacromolecules*, *11*, 3275–3289.

Blazek, J., & Gilbert, E. P. (2011). Application of small-angle X-ray and neutron scattering techniques to the characterisation of starch structure: A review. *Carbohydrate Polymers*, *85*, 281–293.

Brenner, A. M., Adkins, B. D., Spooner, S., & Davis, B. H. (1995). Porosity by small-angle X-ray scattering (SAXS): Comparison with results from mercury penetration and nitrogen adsorption. *Journal of Non-Crystalline Solids*, *185*, 73–77.

Buleon, A., Colonna, P., Planchot, V., & Ball, S. (1998). Starch granules: Structure and biosynthesis. *International Journal of Biological Macromolecules*, *13*, 93–112.

Cameron, R. E., & Donald, A. M. (1992). A small-angle X-ray scattering study of the annealing and gelatinization of starch. *Polymer*, *33*, 2628–2636.

Daniels, D. R., & Donald, A. M. (2003). An improved model for analysing the small angle X-ray scattering of starch granules. *Biopolymers*, *69*, 165–175.

Doutch, J., Bason, M., Franceschini, F., James, K., Clowes, D., & Gilbert, E. P. (2012). Structural changes during starch pasting using simultaneous Rapid Visco Analysis and small-angle neutron scattering. *Carbohydrate Polymers*, *88*, 1061–1071.

Fan, L., Degen, M., Bendle, S., Grupido, N., & Ilvasky, J. (2010). The absolute calibration of a small-angle scattering instrument with a laboratory source. *Journal of Physics Conference Series*, *247*, 012005.

Gallant, D. J., Bouchet, B., & Baldwin, P. M. (1997). Microscopy of starch: Evidence of a new level of granule organisation. *Carbohydrate Polymers*, *32*, 177–191.

Gilbert, E. P., Schulz, J. C., & Noakes, T. J. (2006). 'Quokka' – the small-angle neutron scattering instrument at OPAL. *Physica B*, *385–386*, 1180–1182.

Huber, K. C., & BeMiller, J. N. (2000). Channels of maize and sorghum starch granules. *Carbohydrate Polymers*, *41*, 269–276.

Ilavsky, J., & Jemian, P. R. (2009). Irena: Tool suite for modelling and analysis of small-angle scattering. *Journal of Applied Crystallography*, *42*, 347–353.

Jane, J.-L., Kasemsuwan, T., Leas, S., Zobel, H., & Robyt, J. F. (1994). Anthology of starch granule morphology by scanning electron microscopy. *Starch*, *46*, 121–129.

Kline, S. (2006). Reduction and analysis of SANS and USANS data using IGOR pro. *Journal of Applied Crystallography*, *39*, 895–900.

Oostergetel, G. T., & van Bruggen, E. J. F. (1993). The crystalline domains in potato starch granules are arranged in a helical fashion. *Carbohydrate Polymers*, *21*, 7–12.

Perez, S., & Bertoft, E. (2010). The molecular structures of starch components and their contribution to the architecture of starch granules: A comprehensive review. *Starch – Stärke*, *62*, 389–420.

Perry, P. A., & Donald, A. M. (2000). The role of plasticization in starch granule assembly. *Biomacromolecules*, *3*, 424–432.

Perry, P. A., & Donald, A. M. (2002). The effect of sugars on the gelatinisation of starch. *Carbohydrate Polymers*, *49*, 155–165.

Radlinski, A. P., Mastalerz, M., Hinde, A. L., Hainbuchner, M., Rauch, H., Baron, M., et al. (2004). Application of SAXS and SANS in evaluation of porosity, pore size distribution and surface area of coal. *International Journal of Coal Geology*, *59*, 245–271.

Sujka, M., & Jamroz, J. (2010). Characteristics of pores in native and hydrolysed starch granules. *Starch*, *62*, 229–235.

Szymonska, J., & Krok, F. (2003). Potato starch granule nanostructure studied by high resolution non-contact AFM. *International Journal of Biological Macromolecules*, *33*, 1–7.

Tang, T., Mitsunaga, T., & Kawamura, Y. (2005). Molecular arrangement in blocklets and starch granule architecture. *Carbohydrate Polymers*, *63*, 555–560.

Waigh, T. A., Gidley, M. J., Komanshek, B. U., & Donald, A. M. (2000). The phase transformations in starch during gelatinisation: A liquid crystalline approach. *Carbohydrate Research*, *328*, 165–176.

Wang, S., Blazek, J., Gilbert, E. P., & Copeland, L. (2012). New insights on the mechanism of acid degradation of pea starch. *Carbohydrate Polymers*, *87*, 1941–1949.

Wellner, N., Georget, D. M. R., Parker, M. L., & Morris, V. J. (2011). In situ Raman microscopy of starch granule structures in wild type and *ae* mutant maize kernels. *Starch – Stärke*, *63*, 128–138.